JOURNAL OF COLLOID AND INTERFACE SCIENCE 165, 169–176 (1994)

Kinetics of Cr(III) Adsorption/Desorption at the γ-Al_2O_3/Water Interface by the Pressure-Jump Technique

KUEN-SEN CHANG,* CHENG-FANG LIN,*,[1] DAR-YUAN LEE,† SHANG-LIEN LO,* AND TATSUYA YASUNAGA*,[2]

*Graduate Institute of Environmental Engineering, National Taiwan University, Taipei, Taiwan, 106; and †Graduate Institute of Agricultural Chemistry, National Taiwan University, Taipei, Taiwan, 106

Received January 29, 1993; accepted January 13, 1994

Mechanistic information regarding Cr(III) adsorption onto γ-Al_2O_3 was obtained using the triple layer model (TLM) in conjunction with experimental data gathered using the pressure-jump technique. Adsorption data and TLM simulation results suggest the formation of both mono- and bidentate inner-sphere Cr^{3+} or $CrOH^{2+}$ complexes at the surface of γ-Al_2O_3. The mechanism of Cr(III) sorption was interpreted as proton release from surface hydroxyl group(s) followed by the attachment of Cr^{3+} or $CrOH^{2+}$ to form bidentate $(SO)_2Cr^+$ and monodentate $SOCrOH^+$. The binding constant of Cr^{3+} or $CrOH^{2+}$ with deprotonated reacting site(s) simulated using the TLM and equilibrium sorption data was in excellent agreement with that determined from kinetic results, verifying the proposed reaction mechanisms.

INTRODUCTION

In natural environments, the fate and distribution of metal ions are regulated, in part, via adsorption/desorption and precipitation reactions occurring at the interface between the aqueous solution and minerals such as Fe and/or Al oxides and hydroxides (1, 2). A variety of models has been used to describe the interactions of metal ions and minerals, e.g., the surface complexation model (SCM) by Stumm *et al.* (3) and the triple layer model (TLM) of Leckie and colleagues (4, 5). In general, those models provide a basis for interpreting experimental data; however, the amount of direct evidence available to verify the reaction mechanism is very limited.

Direct information about the surface structure in adsorptive systems can be obtained using the extended X-ray absorption fine structure analysis technique. This technique was employed by Hayes *et al.* (6) to examine selenite and selenate interactions with goethite. Their work provided evidence for the existence of both outer-sphere (selenate) and inner-sphere (selenite) surface complexes, as envisioned in the TLM.

[1] To whom correspondence should be addressed.

[2] Visiting scholar.

Kinetic methods can be used to obtain information regarding reaction steps and mechanisms. Most traditional batch and flow methods are incapable of providing detailed information regarding processes at the interface, owing to the absence of methods that can detect changes in the system as rapidly as the adsorption reaction proceeds. Relaxation methods, especially the pressure-jump technique, have therefore been applied to study some such systems, e.g., sorption of Pb, Zn, Cu, Co, and Mn ions on aluminum oxide and of anions on goethite (7–11). The kinetic and mechanistic behavior of Cr(III) sorption on aluminum oxides has not yet been extensively investigated.

This study presents the equilibrium and kinetics of Cr(III) sorption onto γ-Al_2O_3. Chromium is commonly used in acid electroplating, tanning, painting, dye and drug manufacturing, and petroleum refining (12). The health and environmental effects of carcinogenic Cr(VI) are well known (13–15). If Fe(II), HSO_3^-, or another electron donor such as organic matter is present, Cr(VI) can be reduced to Cr(III), which tends to be attenuated in soil by inorganic phases such as phyllosilicates and hydroxides (16, 17).

Cr(III) ions have unusually slow ligand exchange reactions and have a strong tendency to polymerize in solution (18–23). Several investigators have studied the interactions of Cr(III) with Fe/Al oxide surfaces. Leckie *et al.* (23) proposed that $CrOH^{2+}$ sorbs at the water/goethite interface as a monodentate surface complex. Wehrli *et al.* (18) studied the adsorption kinetics of Cr(III) onto aluminum oxide and reported that Cr(III) sorption is a two-step process and that the resulting surface species included bidentate Cr^{3+}, monodentate $CrOH^{2+}$, and bidentate $CrOH^{2+}$. Karthein *et al.* (22) used electron spin resonance (ESR) and electron spin-echo spectroscopy (ESEEM) to explore the interactions of Cr(III) complexes ($Cr(oxalate)_3^{3+}$) with hydrous δ-Al_2O_3 and reported the formation of inner-sphere, bidentate adsorption complexes of the forms $(SO)_2Cr^+$, $(SO)_2Cr(C_2O_4)^-$, and $(SO)_2Cr(C_2O_4)_2^{3-}$.

The results of the present study extend the current knowledge about the complicated adsorption behavior of trivalent Cr(III) onto γ-Al_2O_3. The main objective of this work was

0021-9797/94 $6.00

to explore the interaction of Cr(III) and γ-Al_2O_3 using the pressure-jump technique. Specifically, the overall equilibrium partitioning between Cr(III) and γ-Al_2O_3 is described. The kinetic rate constants and mechanistic information regarding Cr(III) adsorption at the γ-Al_2O_3/water interface were determined using the relaxation method in conjunction with the TLM.

MATERIALS AND METHODS

Materials

All chemicals used in this study were of reagent analytical grade. The stock Cr(III) solution (1×10^{-2} *M* and pH < 2.9) was prepared by using $Cr(NO_3)_3 \cdot 9H_2O$ and deionized water (Milli-Q). Under these acidic conditions, the formation of Cr(III) polynuclear hydroxo species is not favorable (24). The background electrolyte solutions were adjusted to 0.01, 0.05, and 0.1 *M* using $NaNO_3$. The γ-Al_2O_3 obtained from Aerosil Co. (Japan) was first prewashed with 0.1 *M* NaOH, according to the procedure described by Hohl and Stumm (25). After the prewash, the γ-Al_2O_3 was rinsed with deionized water and dialyzed before use in adsorption experiments.

Experiments

In batch equilibrium experiments, the pH of a suspension containing 3×10^{-3} *M* total Cr(III) and γ-Al_2O_3 (40 g dm^{-3}) was adjusted with concentrated HNO_3 or NaOH to various values in the pH range 3.0–5.0. At each adjusted pH point, a 30-ml suspension was transferred to a polypropylene tube. The pH values of the suspensions were monitored for at least 72 h under an N_2 atmosphere. Once all obvious fluctuation in suspension pH ceased, a further 48-h shaking period under an N_2 atmosphere was performed to ensure that equilibrium was achieved (18). Thereafter, the pH of each suspension was measured, and the solid and liquid were separated by filtration (0.22 μm, Millipore). The filtrate was acidified for subsequent Cr analysis (atomic absorption, Perkin–Elmer 5000).

For the kinetic experiments, the suspensions prepared in the batch equilibrium experiments were transferred to the sample cell of the pressure-jump apparatus. The temperature was maintained at 25 ± 0.1°C in both the sample cell and the reference cell (KCl solution). The pressure-jump apparatus was equipped with a conductivity detector and was similar to that used previously by Inoue *et al.* (26). The primary components of the pressure-jump apparatus were the pressure chamber (Photo High Pressure Inc., Japan), Wheatstone bridge circuit (Sea Land Electr. Wave Inc., Japan), and a digital storage oscilloscope (TEK 2224).

In the pressure-jump relaxation experiments, the equilibrium state of the Cr(III)/γ-Al_2O_3 system was perturbed by raising the system pressure to 100 atm, using a camshaft pressure pump. The high pressure in the autoclave sample cell was transmitted to the suspension through a plastic membrane located on the cell cap. A piece of brass shimstock was used for pressure control. When the pressure in the autoclave became high enough, the shimstock burst, and the pressure returned to the ambient condition within 100 μs. At the moment when the shimstock burst, an oscilloscope was triggered to record the changes in system conductivity. The signals recorded by the oscilloscope were digitized and analyzed by a linear regression technique for calculating the reciprocal relaxation time (τ^{-1}). The correlation coefficient (r^2) was required to be greater than 0.92 in order for the computed τ^{-1} to be acceptable.

Model Analysis

A modified TLM was used to simulate the equilibrium distribution of background electrolyte ions and Cr(III) species at the γ-Al_2O_3/water interface. In the modified TLM, metal ions are allowed to form either inner- or outer-sphere surface complexes, and the effect of surface potential upon solution activity is incorporated into the activity coefficient relationship with a single exponential term. The intrinsic reaction constants and other parameters used in the TLM are summarized in Table 1. Part I (Eqs. [1] and [2]) of Table 1 describes protonation of reacting surface sites, and Part II (Eqs. [3] and [4]) describes the formation of complexes between the background electrolyte ions and the surface. Based on previous work by other investigators (18, 22, 23), the interactions of Cr(III) on the surface of γ-Al_2O_3 are assumed to be those shown in Parts III and IV of Table 1. Ion-pair formation at the β-plane (Eqs. [5] and [6]) occurs if Cr^{3+} or a Cr(III) hydrolytic complex reacts with SOH similarly to a background electrolyte. If adsorption of Cr^{3+} or Cr(III) hydrolytic complex is visualized as a chemically specific reaction, the reaction can be expressed as an inner-sphere surface coordination process (Eqs. [7]–[10]). The equilibrium and mass balance equations are solved simultaneously in the TLM. The specific surface area of γ-Al_2O_3 is 100 m^2/g, according to the manufacturer. Site density was reported by Peri (27) to be 8 sites/nm^2. Inner- and outer-plane capacitances were assumed to be 80 and 20 $\mu F/cm^2$, respectively, as reported by Hayes *et al.* (28). The above parameters were used in the model analysis to determine the best-fit intrinsic constants for the Cr(III)/γ-Al_2O_3 reaction.

RESULTS AND DISCUSSIONS

Figure 1 shows Cr(III) sorption onto γ-Al_2O_3 as a function of pH under various background electrolyte concentrations (0–0.1 *M*). Over a range of less than two pH units, sorption of Cr(III) changes from a negligible amount (at pH 3.1) to nearly total removal (at pH 4.8). The effect of background electrolyte concentration on the adsorption of Cr(III) is fairly insignificant. The formation of different inner- and outer-

TABLE 1
TLM Reactions and Equilibrium Expressions for Cr(III) Species

Reaction (equation)	Instrinsic equilibrium expression/constant	
(I) Surface protolysis reactions		
$SOH_2^+ = SOH + H^+$	$K_{a1}^{int} = \frac{\overline{[SOH]}\,\overline{[H^+]}}{\overline{[SOH_2^+]}} \exp\left(\frac{-\Psi_0 F}{RT}\right) = 10^{-7.2}$	[1]
$SOH = SO^- + H^+$	$K_{a2}^{int} = \frac{\overline{[SO^-]}\,\overline{[H^+]}}{\overline{[SOH]}} \exp\left(\frac{-\Psi_0 F}{RT}\right) = 10^{-9.5}$	[2]
(II) Electrolyte surface reations		
$SOH + Na^+ = SO^- - Na^+ + H^+$	$K_{Na^+}^{int} = \frac{\overline{[SO^- - Na^+]}\,\overline{[H^+]}}{\overline{[SOH]}\,\overline{[Na^+]}} \exp\left[\frac{(\Psi_\beta - \Psi_0)F}{RT}\right] = 10^{-9.1}$	[3]
$SOH + H^+ + NO_3^- = SOH_2^+ - NO_3^-$	$K_{NO3}^{int} = \frac{\overline{[SOH_2^+ - NO_3^-]}}{\overline{[SOH]}\,\overline{[H^+]}\,\overline{[NO_3^-]}} \exp\left[\frac{(\Psi_0 - \Psi_\beta)F}{RT}\right] = 10^{8.7}$	[4]
(III) Outer-sphere surface reactions		
$SOH + Cr^{3+} = SO^- - Cr^{3+} + H^+$	$K_{Cr}^{int} = \frac{\overline{[SO^- - Cr^{3+}]}\,\overline{[H^+]}}{\overline{[SOH]}\,\overline{[Cr^{3+}]}} \exp\left[\frac{(3\Psi_\beta - \Psi_0)F}{RT}\right]$	[5]
$SOH + Cr^{3+} + H_2O = SO^- - CrOH^{2+} + 2H^+$	$K_{Cr}^{int} = \frac{\overline{[SO^- - CrOH^{2+}]}\,\overline{[H^+]}^2}{\overline{SOH}\,\overline{[Cr^{3+}]}} \exp\left[\frac{(2\Psi_\beta - \Psi_0)F}{RT}\right]$	[6]
(IV) Inner-sphere surface reations		
$SOH + Cr^{3+} = SOCr^{2+} + H^+$	$K_{Cr1}^{int} = \frac{\overline{[SOCr^{2+}]}\,\overline{[H^+]}}{\overline{[SOH]}\,\overline{[Cr^{3+}]}} \exp\left(\frac{2\Psi_0 F}{RT}\right)$	[7]
$2SOH + Cr^{3+} = (SO)_2Cr^{2+} + 2H^+$	$K_{Cr2}^{int} = \frac{\overline{[(SO)_2Cr^{2+}]}\,\overline{[H^+]}^2}{\overline{[SOH]}^2\,\overline{[Cr^{3+}]}} \exp\left(\frac{\Psi_0 F}{RT}\right)$	[8]
$SOH + Cr^{3+} + H_2O = SOCrOH^+ + 2H^+$	$K_{CrOH1}^{int} = \frac{\overline{[SOCrOH^+]}\,\overline{[H^+]}^2}{\overline{[SOH]}\,\overline{[Cr^{3+}]}} \exp\left(\frac{\Psi_0 F}{RT}\right)$	[9]
$2SOH + Cr^{3+} + H_2O = (SO)_2CrOH + 3H^+$	$K_{CrOH2}^{int} = \frac{\overline{[(SO)_2CrOH]}\,\overline{[H^+]}^3}{\overline{[SOH]}^2\,\overline{[Cr^{3+}]}}$	[10]

sphere complexes of Cr(III) as proposed in Eqs. [5]–[10] was modeled using the Cr(III) adsorption data with no $NaNO_3$ addition. The formation of ion-pair-like outer-sphere complexes of $SO–Cr^{2+}$ in Eq. [5] or $SO–CrOH^+$ in Eq. [6] was ruled out since the simulation was unable to match the measured pH-adsorption curves (figure not shown).

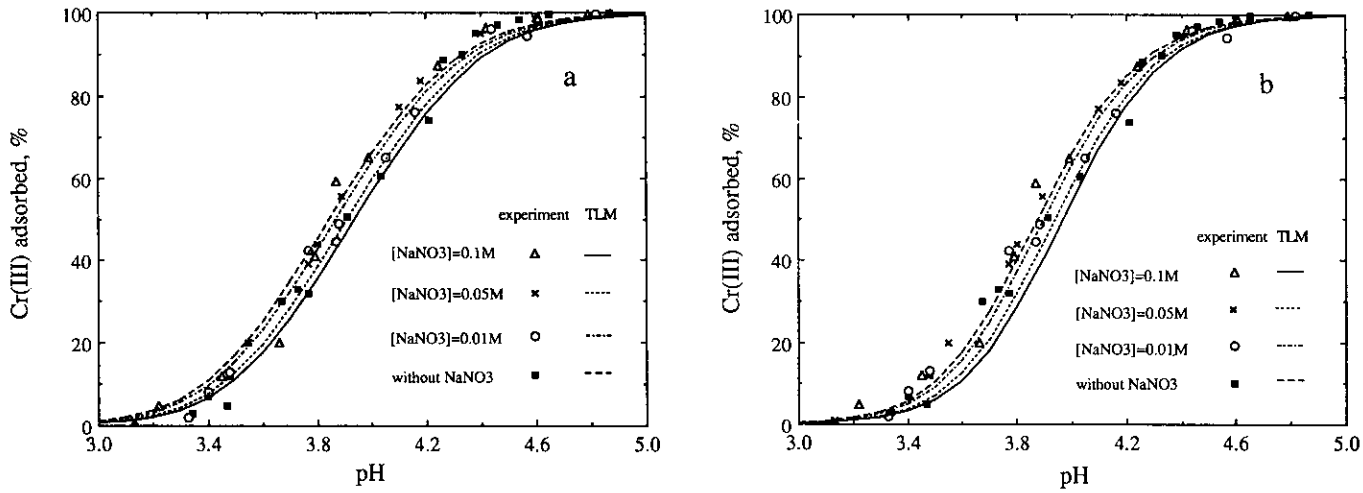

FIG. 1. Adsorption of Cr(III) onto γ-Al_2O_3 as a function of pH under various background $NaNO_3$ concentrations. Solid and dashed lines denote TLM results. (a) Simulation of monodentate $SOCr^{2+}$ using Eq. [7]. (b) Simulation of bidentate $(SO)_2Cr^+$ using Eq. [8] in Table 1. Symbols denote experimental data.

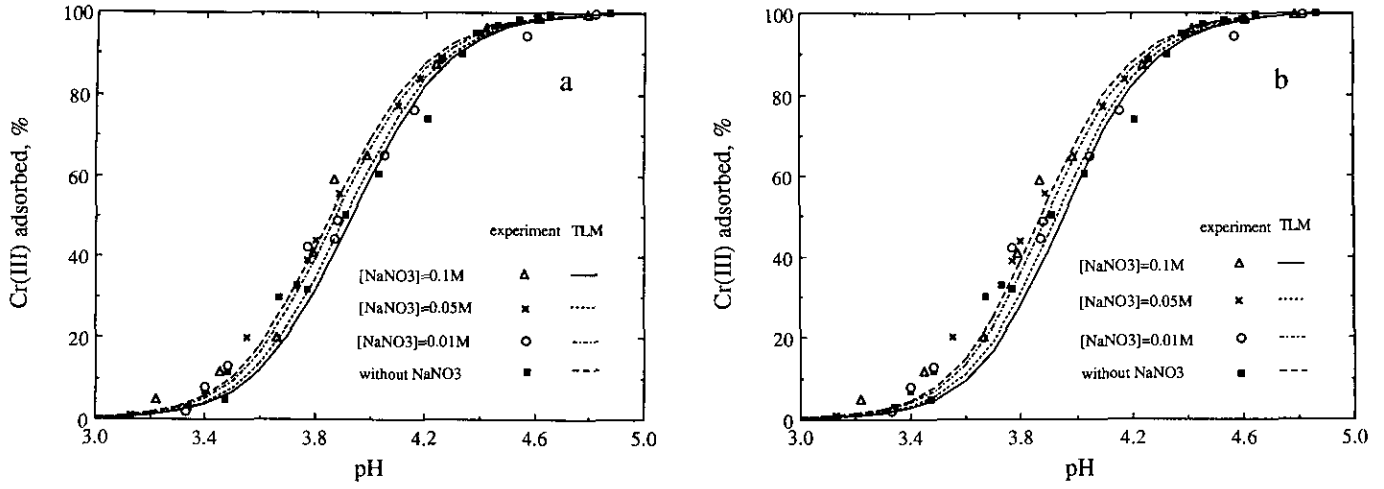

FIG. 2. Adsorption of Cr(III) onto γ-Al_2O_3 as a function of pH under various background $NaNO_3$ concentrations. Solid and dashed lines denote TLM results. (a) Simulation of monodentate $SOCrOH^+$ using Eq. [9]. (b) Simulation of bidentate $(SO)_2CrOH$ using Eq. [10] in Table 1. Symbols denote experimental data.

If it was assumed that the monodentate complex $SOCr^{2+}$ (Eq. [7]) and the bidentate complex $(SO)_2Cr^+$ (Eq. [8]) formed, the model was able to fit the experimental data quite well (Fig. 1). As the major species in solution over the adsorption pH range are Cr^{3+} and $CrOH^{2+}$, the formation of monodentate and bidentate Cr(III) hydrolysis species ($SOCrOH^+$ (Eq. [9]) and $(SO)_2CrOH$ (Eq. [10])) was also simulated. The model was once again able to fit the experimental data quite well, as shown in Fig. 2.

The negligible effect of background electrolyte concentration on the binding of Cr(III) has been attributed to the formation of inner-sphere surface complexes (5, 29), which is consistent with the simulations shown in Figs. 1 and 2. The formation of all four types of Cr(III) complexes with γ-Al_2O_3 surface was also simulated using the TLM. Figure 3 presents the simulation results, and Table 2 summarizes the respective intrinsic formation constants and the distribution of Cr species at pH 4 and 4.8. The results indicate that bidentate Cr^{3+} and monodentate $CrOH^{2+}$ are the likely dominant species.

Wehrli *et al.* reported that Kurbatov plots indicate that slightly more than two protons are released per Cr(III) adsorbed in the reaction of Cr(III) with aluminum oxide (18). The work of Leckie *et al.* supported the stoichiometric relationship of two protons released with one Cr(III) ion sorbed for $CrOH^{2+}$ adsorption (23). The identity of surface species cannot be proven unequivocally by equilibrium adsorption data and the TLM. However, the stoichiometric relationship and TLM modeling of the Cr(III)/aluminum oxide reaction suggest the formation of bidentate Cr^{3+} or monodentate $CrOH^{2+}$ surface complexes and the presence, at lower concentrations, of monodentate Cr^{3+} and bidentate $CrOH^{2+}$ surface complexes.

Cr(III) aquo ions have a strong tendency to form polynuclear hydroxo species under specific solution conditions (19–21). Karthein *et al.* employed ESR and ESEEM to study the interaction of Cr(III) complexes with hydrous δ-Al_2O_3 under conditions of total Cr(III) up to 3×10^{-3} M and pH 4.2 and reported that "chromium complexation at specific surface sites rather than chromium polymer formation takes place" (22). The formation of a bidentate $(SO)_2Cr(H_2O)_4^+$ surface complex was postulated. An X-ray absorption spectroscopic study of the sorption of Cr(III) at the oxide–water interface conducted by Charlet and Manceau (30) showed that small hydroxy polymers might be present at the surface when the Cr(III) surface coverage exceeded about 10% of the active sites. In this work, the Cr(III) sorption density on γ-Al_2O_3 for all the surface species (Eq. [7]–[10]) proposed is calculated to be less than 8% of the total number of reacting sites. Furthermore, the rate of Cr^{3+} dimer and trimer formation is much less than the rate of Cr(III)

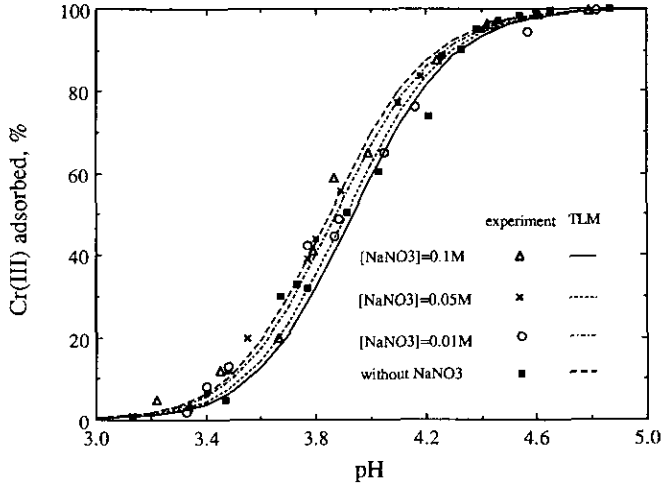

FIG. 3. TLM simulation of mono-/bidentates Cr^{3+} and $CrOH^{2+}$ using Eqs. [7]–[10] in Table 1. Symbols denote experimental data.

TABLE 2
Optimized Intrinsic Formation Contants and Complexed Cr(III) Concentrations from the Simulation of Mono- and Bidentate Formations of Cr^{3+} and $CrOH^{2+}$ Species

Species	$SOCr^{2+}$	$(SO)_2Cr^+$	$SOCrOH^+$	$(SO)_2CrOH$	Reacted SOH sites/ Total SOH sites[a]
log K^{int}	6.0	−0.54	−1.75	−10.0	—
pH 4	2.0×10^{-4} M	7.0×10^{-4} M	11.1×10^{-4} M	0.8×10^{-4} M	5.4%
pH 4.8	2.4×10^{-4} M	10.1×10^{-4} M	16.1×10^{-4} M	1.3×10^{-4} M	7.7%

[a] Total SOH sites: 5.32×10^{-2} M.

adsorption (22). Therefore, it seems reasonable to discount the formation of Cr(III) polymers on the surface. Based on this assumption, the possible monomeric Cr(III) species sorbed on aluminum oxide were examined by a relaxation method.

A typical relaxation curve is shown in Fig. 4a for the Cr(III)/γ-Al_2O_3 suspension, using the pressure-jump apparatus with an electrical conductivity detector. The signal recorded in the oscilloscope clearly indicates a decrease in suspension conductivity during the relaxation period. The reciprocal relaxation times (τ^{-1}) can be obtained from the net natural logarithmic plot of the electrical potential versus time, as shown in Fig. 4b. Systems containing $Cr(NO_3)_3$ only and the supernatant of the suspension of γ-Al_2O_3 were also subjected to the pressure-jump test using the same process. No relaxation was noticed in either of these systems, demonstrating that relaxation can be attributed solely to the association/dissociation of Cr(III) at the water/γ-Al_2O_3 interface. The measured reciprocal relaxation times (τ^{-1}) between pH 4 and 4.6 are shown in Fig. 5; τ^{-1} increases with an increase in suspension pH. This trend is consistent with those for other metals (e.g., Pb, Zn, etc.) reported previously (7, 8). The measured τ^{-1} values, suspension pH, ionic strength, activity coefficients, and the percentage of Cr(III) adsorbed, are presented in Table 3.

Proposed reaction pathways in the Cr(III)/γ-Al_2O_3 system are presented in Table 4. Formation of bidentate Cr^{3+} and monodentate $CrOH^{2+}$ complexes (corresponding to Mechanisms I–IV) were examined. The fast mechanistic pathway proposed by Hachiya *et al.* (8) and Hayes (31) in which the adsorption process is described as an associative mechanism with respect to the exchanged proton is presented as Mechanisms I and II in Table 4. Different possible mechanistic pathways for the adsorption processes were formulated as proton release from surface hydroxyl group(s) followed by attachment of Cr(III) species, as shown in Mechanisms III and IV.

In order to examine the plausibility of the proposed adsorption mechanisms, the corresponding reciprocal relaxation time constants were derived as a function of the reactant

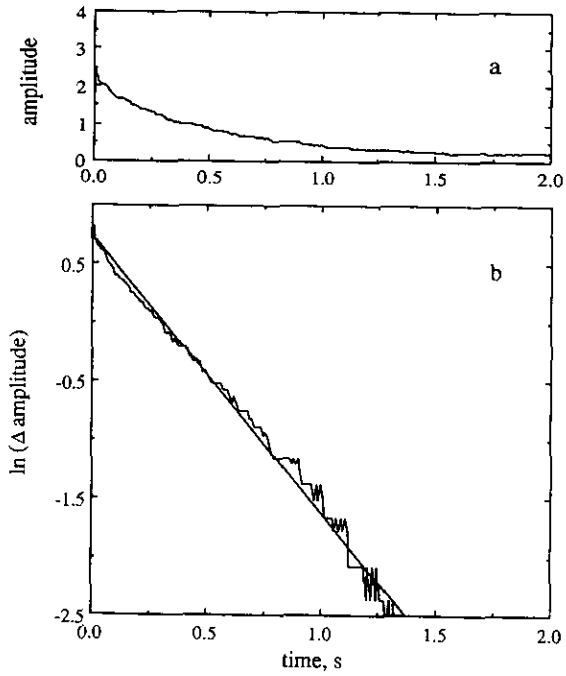

FIG. 4. (a) Typical relaxation curve in Cr(III)/γ-Al_2O_3 system by the pressure-jump technique at pH 4.32, sweep 0.2 s/div and 25°C. (b) Net natural logarithmic plot of the typical relaxation curve.

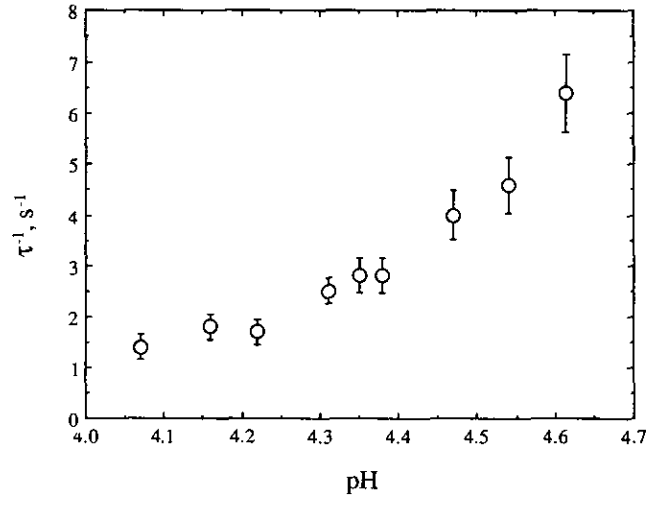

FIG. 5. The pH dependence of reciprocal relaxation time. System contains [γ-Al_2O_3] = 40 g liter^{-1}, $[Cr(III)]_T = 3 \times 10^{-3}$ M at 25°C.

TABLE 3
Reciprocal Relaxation Time, Ionic Strength, Ionic Activity, and Chromium (III) Adsorption as a Function of pH in the Cr(III)/γ-Al_2O_3 System

pH	τ^{-1} (s^{-1})	I (10^{-3} M)	γ (H^+)	γ (Cr^{3+})	γ ($CrOH^{2+}$)	$[Cr(III)]_{ads}$ (%)
4.07	1.4	4.28	0.938	0.588	0.774	77
4.16	1.8	3.43	0.943	0.592	0.792	84
4.22	1.7	3.01	0.946	0.608	0.802	88
4.31	2.5	2.59	0.949	0.627	0.813	93
4.35	2.8	2.49	0.950	0.633	0.816	94
4.38	2.8	2.41	0.951	0.636	0.818	95
4.47	4.0	2.28	0.952	0.644	0.822	97
4.54	4.6	2.22	0.952	0.647	0.824	98
4.62	6.4	2.20	0.953	0.648	0.824	99

and product concentrations ({MI*}, {MII*}, {MIII*}, and {MIV*}) for the postulated mechanisms. These constants are also summarized in Table 4. If a plot of τ^{-1} measured from the pressure-jump experiments against the corresponding "{M*}" function calculated from the TLM is linear, the hypothesized mechanism is consistent with the data. The intrinsic reaction rate constant(s) can be determined from the slope or/and intercept of such a plot. Based on such a test, Mechanisms I and II (the Hachiya mechanism) were ruled out, since the corresponding plots were not linear.

Plots of experimentally determined τ^{-1} values versus {MIII*} and {MIV*} were linear (Figs. 6 and 7), and the slopes and intercepts of the straight lines were used to compute the forward and reverse rate constants of relevant reactions. The intrinsic adsorption equilibrium constants calculated from the kinetic experiments (i.e., the ratio of the forward and reverse reaction rate constants) and the equilibrium constants simulated from the TLM are listed in Table 5. The equilibrium constants obtained from kinetic experiments (for $(SO)_2Cr^+$, and $SOCrOH^+$ species) are in good agreement with those from equilibrium and the TLM work, indicating that Mechanisms III and IV are reasonable models for the reactions in the Cr(III)/γ-Al_2O_3 system. The results are consistent with the findings of Karthein *et al.* (22).

Wehrli *et al.* discussed the adsorption kinetics of Cr(III) on δ-Al_2O_3 in batch systems (18). The intrinsic adsorption rate constant of divalent metal ions and their water exchange rates are closely correlated by a linear free-energy relationship (8, 18). Their work suggested that intrinsic adsorption rate constants can be calculated from the water exchange rates of the aquo metal ions. The loss of one water molecule from a metal ion species was believed to be the rate-limiting step for metal sorption. By comparing the water exchange rates of Cr^{3+} and $CrOH^{2+}$ [k_{-w} of $CrOH^{2+}$ is about two orders of magnitude faster (32)] with experimental observations of

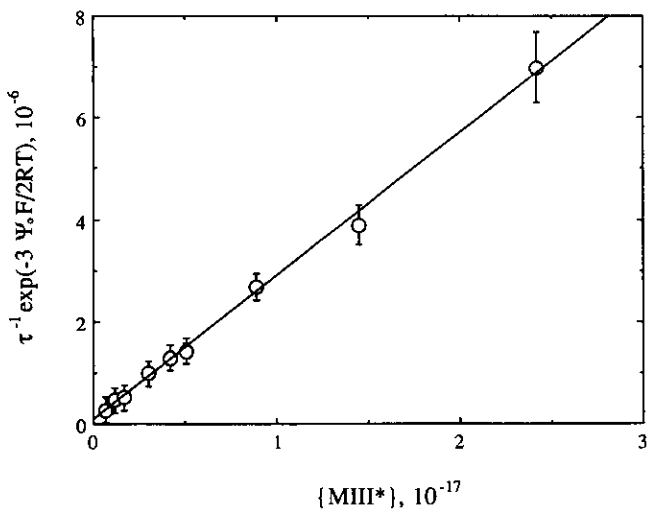

FIG. 6. Plot of $\tau^{-1}\exp(-3\Psi_0F/2RT)$ vs {MIII*} in Eq. [16]. The concentrations of Cr(III) species were calculated based on the optimized intrinsic formation constants listed in Table 2.

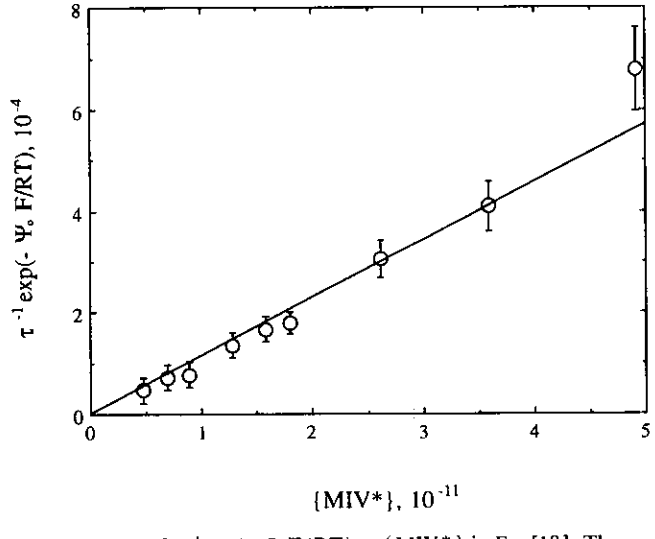

FIG. 7. Plot of $\tau^{-1}\exp(-\Psi_0F/RT)$ vs {MIV*} in Eq. [18]. The concentrations of Cr(III) species were calculated based on the optimized intrinsic formation constants listed in Table 2.

TABLE 4

Possible Mechanistic Pathways and the Relationship between Reciprocal Relaxation Times and Concentrations of Cr(III) Species on a γ-Al_2O_3 Surface

Mechanism I

(1) Mechanistic pathway

$$2\text{SOH} \underset{k_{-1}}{\overset{k_1}{\rightleftharpoons}} 2\text{SOH}\cdots\text{Cr}^{3+} \underset{k_{-2}}{\overset{k_2}{\rightleftharpoons}} (\text{SO})_2\text{Cr}^{+} + 2\text{H}^{+} \qquad [11]$$

(2) Relationship between reciprocal relaxation times and species activities

$$\tau^{-1} = k_1^{\text{int}}\left\{\exp\left(\frac{-3\Psi_0 F}{2RT}\right)([\overline{\text{SOH}}]^2 + [\overline{\text{SOH}}]\{\overline{\text{Cr}^{3+}}\}) + \frac{1}{K^{\text{int}}}\exp\left(\frac{-\Psi_0 F}{2RT}\right)([\overline{(\text{SO})_2\text{Cr}^{+}}]\{\overline{\text{H}^{+}}\} + \{\overline{\text{H}^{+}}\}^2)\right\} = k_1^{\text{int}}\{\text{MI}^*\} \qquad [12]$$

Mechanism II

(1) Mechanistic pathway

$$\text{SOH} \underset{k_{-1}}{\overset{k_1}{\rightleftharpoons}} \text{SO}\cdots\text{CrOH}^{2+} \underset{k_{-2}}{\overset{k_2}{\rightleftharpoons}} \text{SOCrOH}^{+} + \text{H}^{+} \qquad [13]$$

(2) Relationship between reciprocal relaxation times and species activities

$$\tau^{-1} = k_1^{\text{int}}\left\{\exp\left(\frac{-\Psi_0 F}{RT}\right)([\overline{\text{SOH}}] + \{\overline{\text{CrOH}^{2+}}\}) + \frac{1}{K^{\text{int}}}([\overline{\text{SOCrOH}^{+}}] + \{\overline{\text{H}^{+}}\})\right\} = k_1^{\text{int}}\{\text{MII}^*\} \qquad [14]$$

Mechanism III

(1) Mechanistic pathway

$$2\text{SOH} \underset{k_{-1}}{\overset{k_1}{\rightleftharpoons}} 2\text{SO}^{-}\cdots 2\text{H}^{+} \underset{k_{-2}}{\overset{k_2}{\rightleftharpoons}} (\text{SO})_2\text{Cr}^{+} + \text{Cr}^{3+} \qquad [15]$$

(2) Relationship between reciprocal relaxation times and species activities

$$\tau^{-1}\exp\left(\frac{-3\Psi_0 F}{2RT}\right) = k_2^{\text{int}}\left\{\exp\left(\frac{-3\Psi_0 F}{RT}\right)\left([\overline{\text{SO}^{-}}]^2 + \frac{[\overline{\text{SO}^{-}}]\{\overline{\text{Cr}^{3+}}\}}{G}\right)\right\} + k_{-2}^{\text{int}} = k_2^{\text{int}}\{\text{MIII}^*\} + k_{-2}^{\text{int}} \qquad [16]$$

with

$$G \equiv \frac{\overline{\{\text{H}^{+}\}^2[\text{SO}^{-}]}}{(K_{a2}^{\text{int}})^2\exp(2\Psi_0 F/RT)[\overline{\text{SOH}}]+\overline{\{\text{H}^{+}\}[\text{SO}^{-}]}^2} + 1$$

Mechanism IV

(1) Mechanistic pathway

$$\text{SOH} \underset{k_{-1}}{\overset{k_1}{\rightleftharpoons}} \text{SO}^{-}\cdots\text{H}^{+} \underset{k_{-2}}{\overset{k_2}{\rightleftharpoons}} \text{SOCrOH}^{+} + \text{CrOH}^{2+} \qquad [17]$$

(2) Relationship between reciprocal relaxation times and species concentrations

$$\tau^{-1}\exp\left(\frac{-\Psi_0 F}{RT}\right) = k_2^{\text{int}}\left\{\exp\left(\frac{-2\Psi_0 F}{RT}\right)\left([\overline{\text{SO}^{-}}] + \{\overline{\text{CrOH}^{2+}}\}\frac{(K_1^{\text{int}})\exp(\Psi_0 F/RT)+\overline{[\text{SO}^{-}]}}{(K_1^{\text{int}})\exp(\Psi_0 F/RT)+\{\text{H}^{+}\}\overline{[\text{SO}^{-}]}}\right)\right\} + k_{-2}^{\text{int}} = k_2^{\text{int}}\{\text{MIV}^*\} + k_{-2}^{\text{int}} \qquad [18]$$

adsorption kinetics, Wehrli *et al.* (18) suggested the formation of CrOH^{2+} complex with the surface of δ-Al_2O_3 (although the formation of bidentate Cr^{3+} is also fairly likely). In this study, the water exchange rates of Cr^{3+} and CrOH^{2+} were used to estimate the intrinsic adsorption rate constants using the linear free-energy relationship of Wehrli *et al.* There was a significant difference between the calculated rate constants and the rate constant determined by pressure-jump in this work. Similar results were noted in the work of Wehrli *et al.* based on the comparison of the linear free-energy relationship calculated value and their experimental observation. According to Wehrli *et al.*, one explanation for the

TABLE 5
The Intrinsic Rate Constants and Equilibrium Constants in Mechanism III and IV

Mechanism	$\log k_2^{int}$ (L mol^{-1} s^{-1})	$\log k_{-2}^{int}$ (s^{-1})	$\log K_{2,kinetic}^{int}$ (L mol^{-1})	$\log K_{2,equili}^{int}$ (L mol^{-1})
III	11.45[a]	−7.08	18.53[b]	18.46[b]
IV	7.06	−6.20	13.26	11.85

[a] Unit: L^2 mol^{-2} s^{-1}.
[b] Unit: L^2 mol^{-2}.

discrepancy is that the metal center may interact with the surface ligand by coordinating with it before a water molecule is released. In an equivalent solution system, Xu *et al.* have suggested that the complete dissociative loss of an H_2O molecule cannot be the only significant step in the ligand substitution process (32).

SUMMARY

In this work, the pressure-jump technique was used to examine the adsorption kinetics of Cr(III) to γ-Al_2O_3. Although the assumption that $(SO)_2Cr^+$ and $SOCrOH^+$ form yielded excellent agreement between the thermodynamic and kinetic results, our results still suggest that monodentate Cr^{3+} and bidentate $CrOH^{2+}$ might also be present at the interface. Adsorption of Cr(III) onto γ-Al_2O_3 was unaffected by ionic strength changes. The adsorption of Cr(III) onto γ-Al_2O_3 could be interpreted as a two-step process: proton release from surface hydroxyl group(s) (SOH) followed by attachment of Cr(III) to the deprotonated site(s) of the surface complex. The respective intrinsic forward and reverse reaction rate constants for the bidentate Cr^{3+} and monodentate $CrOH^{2+}$ were determined kinetically.

ACKNOWLEDGMENTS

The authors wish to thank Professor Mark M. Benjamin, University of Washington, for the valuable discussions and the reviewers for their constructive comments. Funding for this research was provided by the National Science Council of the Republic of China under Grant NSC 82-0410-E-002-136.

REFERENCES

1. Huang, C. P., and Stumm, W., *J. Colloid Interface Sci.* **34,** 409 (1973).
2. Benjamin, M. M., *Environ. Sci. Technol.* **17,** 686 (1983).
3. Stumm, W., Huang, C. P., and Jenkins, S. R., *Croat. Chem. Acta* **42,** 223 (1970).
4. Davis, J. A., and Leckie, J. O., *J. Colloid Interface Sci.* **67,** 90 (1978).
5. Hayes, K. F., and Leckie, J. O., *J. Colloid Interface Sci.* **115,** 564 (1987).
6. Hayes, K. F., Roe, A. L., Brown, G. E., Hodgson, K. O., Leckie, J. O., and Parks, G. A., *Science* **238,** 783 (1987).
7. Hachiya, K., Ashida, M., Sasaki, M., Kan, H., Inoue, T., and Yasunaga, T., *J. Phys. Chem.* **83,** 1866 (1979).
8. Hachiya, K., Sasaki, M., Saruta, Y., Mikami, N., and Yasunaga, T., *J. Phys. Chem.* **88,** 23 (1984).
9. Zhang, P. C., and Sparks, D. L., *Soil Sci. Soc. Am. J.* **53,** 1028 (1989).
10. Zhang, P. C., and Sparks, D. L., *Soil Sci. Soc. Am. J.* **54,** 1266 (1990).
11. Zhang, P. C., and Sparks, D. L., *Environ. Sci. Technol.* **24,** 1848 (1990).
12. Nieboer, E., and Jusys, A. A., *in* "Chromium in the Natural and Human Environments" (J. O. Nriagu and E. Nieboer, Eds.), p. 25. Wiley, New York, 1988.
13. Davis, J. A., and Leckie, J. O., *J. Colloid Interface Sci.* **74,** 32 (1980).
14. Zachara, J. M., Girvin, D. C., Schmidt, R. L., and Resch, C. T., *Environ. Sci. Technol.* **21,** 589 (1987).
15. Zachara, J. M., Ainsworth, C. E., Cowan, C. E., and Resch, C. T., *Soil Sci. Soc. Am. J.* **53,** 418 (1989).
16. Bartlett, R. L., and Kimble, J. M., *J. Environ. Qual.* **5,** 379 (1976).
17. Schroeder, D. C., and Lee, G. F., *Water, Air, Soil Pollut.* **4,** 355 (1975).
18. Wehrli, B., Ibric, S., and Stumm, W., *Colloids Surf.* **51,** 77 (1990).
19. Stunzi, H., and Marty, W., *Inorg. Chem.* **22,** 2145 (1983).
20. Stunzi, H., Rotzinger, F., and Marty, W., *Inorg. Chem.* **23,** 2160 (1984).
21. Rotzinger, F. P., Stunzi, H., and Marty, W., *Inorg. Chem.* **25,** 489 (1986).
22. Karthein, R., Motschi, H., Schweiger, A., Ibric, S., Sulzberger, B., and Stumm, W., *Inorg. Chem.* **30,** 1606 (1991).
23. Leckie, J. O., Appleton, A. R., Ball, N. B., Hayes, K. F., and Honeyman, B. D., EPRI RP-910-1, Electric Power Research Institute, Palo Alto, CA, 1984.
24. Baes, C. F., and Mesmer, J. R. E., "The Hydrolysis of Cations," p. 211. Wiley, New York, 1976.
25. Hohl, H., and Stumm, W., *J. Colloid Interface Sci.* **55,** 281 (1976).
26. Inoue, T., Chang, K. S., Lin, C. F., and Yasunaga, T., *J. Colloid Interface Sci.* **155,** 325 (1993).
27. Peri, J. B., *J. Phys. Chem.* **69,** 211 (1965).
28. Hayes, K. F., Redden, G., Ela, W., and Leckie, J. O., *J. Colloid Interface Sci.* **142,** 448 (1991).
29. Swallow, K. C., Hume, D. N., and Morel, F. M. M., *Environ. Sci. Technol.* **14,** 1326 (1980).
30. Charlet, L., and Manceau, A. A., *J. Colloid Interface Sci.* **148,** 443 (1992).
31. Hayes, K. F., Ph.D. Dissertation, Stanford University, Stanford, CA, 1987.
32. Xu, F. C., Krouse, J. R., and Swaddle, T. W., *Inorg. Chem.* **24,** 267 (1985).